APPLIED SCIENCES AND ENGINEERING

Ultrafast all-climate aluminum-graphene battery with quarter-million cycle life

Hao Chen, Hanyan Xu, Siyao Wang, Tieqi Huang, Jiabin Xi, Shengying Cai, Fan Guo, Zhen Xu, Weiwei Gao, Chao Gao*

Copyright © 2017 The Authors, some rights reserved; exclusive licensee American Association for the Advancement of Science. No claim to original U.S. Government Works. Distributed under a Creative Commons Attribution NonCommercial License 4.0 (CC BY-NC).

Rechargeable aluminum-ion batteries are promising in high-power density but still face critical challenges of limited lifetime, rate capability, and cathodic capacity. We design a "trihigh tricontinuous" (3H3C) graphene film cathode with features of high quality, orientation, and channeling for local structures (3H) and continuous electron-conducting matrix, ion-diffusion highway, and electroactive mass for the whole electrode (3C). Such a cathode retains high specific capacity of around 120 mAh g^{-1} at ultrahigh current density of 400 A g^{-1} (charged in 1.1 s) with 91.7% retention after 250,000 cycles, surpassing all the previous batteries in terms of rate capability and cycle life. The assembled aluminum-graphene battery works well within a wide temperature range of −40 to 120°C with remarkable flexibility bearing 10,000 times of folding, promising for all-climate wearable energy devices. This design opens an avenue for a future super-batteries.

INTRODUCTION

Aluminum-ion battery (AIB) has significant merits of low cost, nonflammability, and high capacity of metallic aluminum anode based on three-electron redox property. However, due to the inadequate cathodic performance, especially capacity, high-rate capability, and cycle life, AIB still cannot compete with Li-ion batteries and supercapacitors (*1*). The energy density of AIB (40 to 60 Wh kg^{-1}) (*2*, *3*) is much lower than that of commercialized Li-ion battery (150 to 250 Wh kg^{-1}), and its power density (3 to 30 kW kg^{-1}) and cycle life (200 to 25,000 cycles) are obviously lower than those of advanced supercapacitors (30 to 100 kW kg^{-1} and 10,000 to 100,000 cycles) (*2*, *4*). Hence, finding a new design to comprehensively upgrade the cathode performance is of crucial importance.

Graphite, graphene, sulfur, and metal sulfide have been selected as the cathode materials of AIB, of which graphitic carbon is highly promising in terms of fast charging and stable cycling. For a desired carbon-based cathode, four basic requirements should be fulfilled simultaneously: (i) highly crystallized defect-free graphene lattice as active anion intercalation site affording available energy storage capacities (*2*); (ii) continuous electron-conducting matrix for large current transportation and internal polarization mitigation; (iii) high mechanical strength and Young's modulus for preventing material collapsing or disintegrating during repeated anion intercalation and deintercalation (*5*); and (iv) interconnected channels facilitating high electrolyte permeability, ion diffusion, and further fast redox reaction between electrolyte and active material. Previous studies have demonstrated that nonoriented graphitic/graphene foams (*1*, *6*, *7*) and dense natural graphite (*1*, *3*, *8*, *9*) can afford partially decent performance as the cathode of AIB, whereas their cycle life and rate capability are limited mainly because of unsatisfying aforementioned requirements, leading to insufficient cell performance compared with supercapacitors.

To address these issues, we propose a "trihigh tricontinuous (3H3C) design" to achieve the ideal graphene film (GF-HC) cathode with excellent electrochemical performances. Ordered assembling of graphene liquid crystal led to a highly oriented structure satisfying requirement (iii). High temperature annealing and concomitant "gas pressure" contributed to high-quality yet high channeling graphene structure that met requirements (i), (ii), and (iv) simultaneously. Owing to this targeted "3H3C design," the resulting aluminum-graphene battery (Al-GB) achieved ultralong cycle life (91.7% retention after 250,000 cycles), unprecedented high-rate capability (111 mAh g^{-1} at 400 A g^{-1} based on the cathode), wide operation temperature range (−40° to 120°C), unique flexibility, and nonflammability.

RESULTS

Production and characterization of the GF-HC cathode

GF-HC film was fabricated by either cast-coating (*10*) or wet-spinning (*11*) graphene oxide (GO) liquid crystal solution into GO film (*12*), followed by chemical reduction for producing reduced GO (rGO) film (Fig. 1B) and high-temperature annealing. Assembling of GO liquid crystal contributes to highly aligned graphene sheet structure, leading to higher electrical conductivity and mechanical properties than graphene foams composed of nonoriented graphene sheets (*13*). The rGO film was then annealed at 2850°C to restore atomic defects, converting into tens of centimeter-long continuous silvery GF (Fig. 1C). Such a high-quality, highly oriented GF could meet the requirements (i), (ii), and (iii) simultaneously. To access smooth paths for fast transportation of ions and permeation of electrolyte [for example, requirement (iv)], we introduced continuous channels into GF during thermal annealing by using a gas pressure effect caused by deoxygenating reaction (fig. S1A) (*10*, *14*). The in situ gas pressure gave rise to hierarchically connected channels among graphene layers for both horizontal permeation and vertical infiltration. Thus, an ideal GF-HC cathode could be achieved with well-designed trihigh (that is, high quality, high orientation, and high channeling) and tricontinuous (that is, continuous electronic conductor of graphene matrix, continuous electrolyte/ion penetration way of channel network, and continuous active material of few-layered graphene framework) structures (*15*). As a comparison, control GF samples with fewer channels were fabricated, defined as GF-p with 0.2-kPa pressure and GF-Hp with 1-kPa pressure during annealing (see Materials and Methods).

Multiple characterizations demonstrate the successful 3H3C design of GF-HC. Undetectable D band in Raman spectra (Fig. 2A) and neglectable oxygen peak in x-ray photoelectron spectroscopy (XPS) spectra

MOE Key Laboratory of Macromolecular Synthesis and Functionalization, Department of Polymer Science and Engineering, Key Laboratory of Adsorption and Separation Materials and Technologies of Zhejiang Province, Zhejiang University, 38 Zheda Road, Hangzhou 310027, P. R. China.
*Corresponding author. Email: chaogao@zju.edu.cn

Downloaded from http://advances.sciencemag.org/ on January 19, 2021

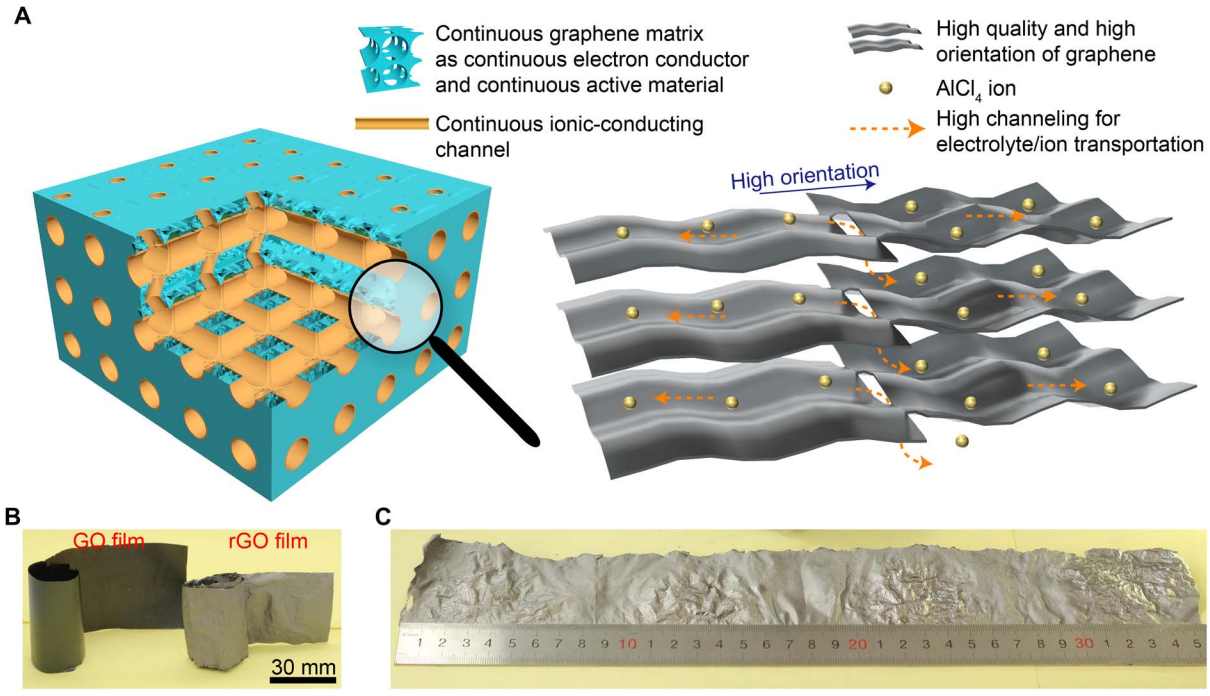


Fig. 1. Cathode material design and preparation. (**A**) Illustration of tricontinuous (3C, continuous electron conductor, continuous ion-conducting channel, and continuous active material) and trihigh (3H, high-quality graphene, high-orientation assembling, and high channeling) design for a desired graphene cathode. (**B**) Photograph of GO and rGO films. (**C**) Photograph of as-prepared silvery GF-HC maintaining its original integrity.

(Fig. 2B and fig. S2) prove the absence of defects in atomic structure of GF-HC, which greatly differ with its highly defective precursors. The high-resolution transmission electron microscopy (HRTEM; Fig. 2C) image and corresponding inverse fast Fourier transform (IFFT; inset in Fig. 2C) pattern also show perfect graphene honeycomb atomic lattice without any sign of disruptive defect sites (*2*). These results demonstrate the "high-quality" feature of GF-HC. In addition, the x-ray diffraction (XRD) spectra exhibit strong characteristic (002) peak at 26.52° (fig. S1C). The distance between graphene sheets is 0.336 nm, as determined by Bragg's equation based on XRD peak position, which is consistent with the distance of around 0.34 nm between eight neighboring few-stacked graphene layers in HRTEM image (Fig. 2D and fig. S3). This few-stack feature of GF-HC makes it greatly different with highly stacked expanded graphite and bulk graphite (*8*) in not only material characteristics (figs. S2, G and H, and S3) but also electrochemical performances.

Scanning electron microscopy (SEM) images illustrate the channeled yet aligned micrometer-sized structure of the GF-HC cathode. Those few-stack graphene sheets were highly aligned along the sheet plane (fig. S4A), suggesting the "high-orientation" feature of GF-HC especially when compared with nonoriented graphene foam (fig. S5). Because of expansion in GF caused by gas pressure (*14*), micrometer-sized gasbags and nano-sized intervals formed between aligned graphene layers to serve as horizontal channels favoring in-plane diffusion of ions (Fig. 2, E and F). Fissures were also created in the surface of GF-HC (Fig. 2G and fig. S4B) to serve as the vertical permeation path for out-plane diffusion of ions, which originated from weak boundaries of graphene sheets in resisting gas pressure. These vertical infiltration fissures, horizontal micrometer-sized gasbags, and nano-sized intervals made up the interconnected three-dimensional (3D) infiltration channels, guaranteeing both "high channeling" and "continuous ionic diffusion channel" features of GF-HC. In comparison, the pressure-tuned GF-p and GF-Hp showed smoother surface with much fewer fissures, gasbags, and intervals (Fig. 2H and figs. S4, D to I, and S5D) as well as lower specific surface area and macroporosity (fig. S6). Such a high channeling GF-HC can afford better permeability for electrolyte infiltration and ion diffusion (*16*). As a result, an $[EMIm]Al_xCl_y$ ionic liquid electrolyte droplet quickly dispersed in (Fig. 2I) and penetrated through GF-HC within 45 min (Fig. 2J); the initial contact angle of dimethyl formamide (DMF) droplet on GF-HC (22.5°) decreased to zero within 18 s due to complete penetration. By contrast, the electrolyte droplet on GF-Hp exhibited neglectable change and no penetration after 18 hours (fig. S7), and the initial contact angle of DMF droplet on GF-p and GF-Hp (both 36°) changed little after 80 s (34° for GF-p and 36° for GF-Hp), indicating poor permeability that failed to meet the critical requirement (iv) for an electrode material. Moreover, these combined merits of ultrathin few-stacked graphene sheets (figs. S2, G and H, and S3) and continuous channel constructed 3D porous yet continuous ionic conducting phase provide GF-HC the "highly continuous active material" feature for fast ion intercalation in the cathode (*15*).

In addition, because of its high orientation, GF-HC also exhibited remarkable flexibility and good mechanical strength (fig. S9) that far surpass nonoriented graphene foam (*17*): Tensile strength of 24.5 MPa at the breakage elongation ratio of 3.92% and a high Young's modulus of 600 MPa. These good mechanical properties of GF-HC reveal its strong resistance against electrode fracture during repeated ion intercalation and deintercalation process, favoring cycling stability (*5*). Regarding vital electronic conductivity, the decimeter-long continuous and highly crystallized GF-HC achieved an impressive value of 270,000 S m^{-1}, far surpassing those of nonoriented graphene foam (1000 to 2000 S m^{-1}) (*17*, *18*), affording a continuous yet ultrahigh electron-conducting matrix.

Downloaded from http://advances.sciencemag.org/ on January 19, 2021

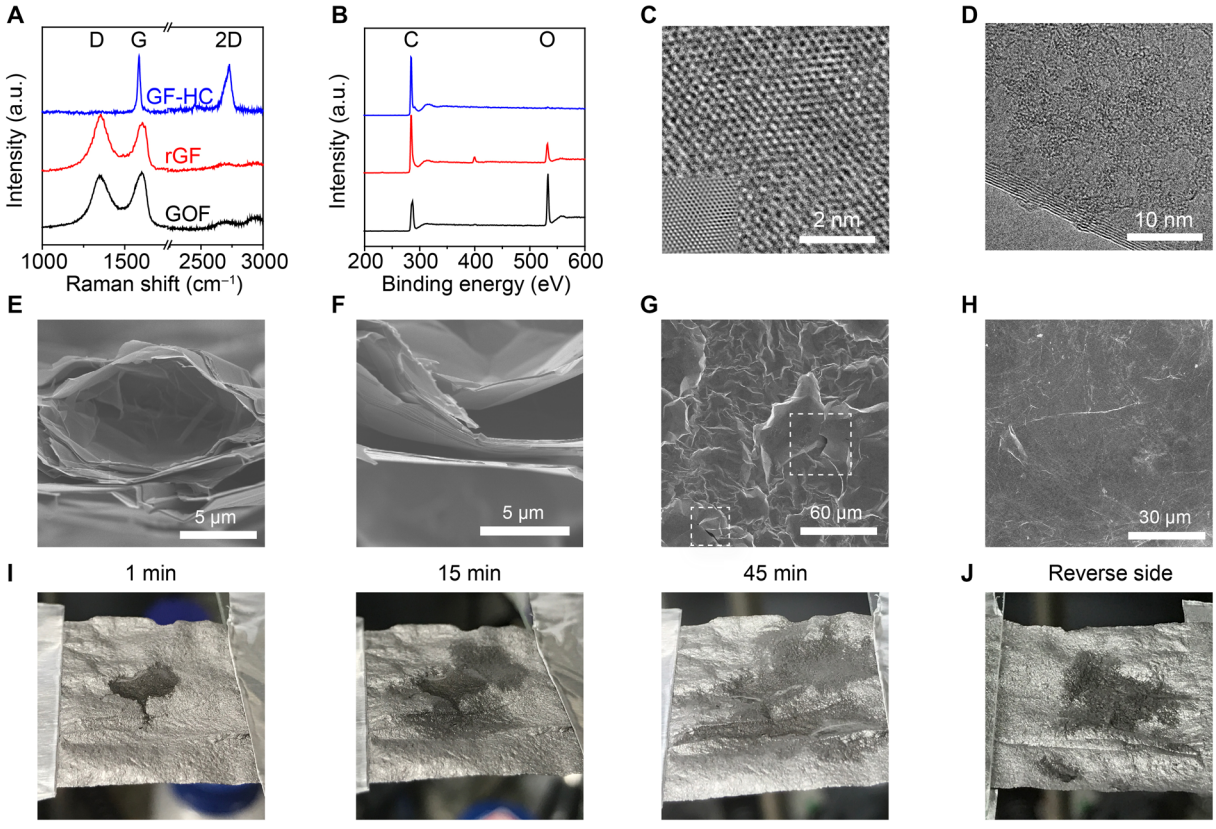


Fig. 2. Structure of the GF cathode. (**A**) Raman spectra of GO film (GOF), rGO film (rGF), and GF-HC exhibiting a decreasing ratio of peak intensity (I_D/I_G) from 0.94 for GOF and 1.17 for rGF to 0 for defect-free GF-HC. a.u., arbitrary units. (**B**) XPS spectra of GOF, rGF, and GF-HC exhibiting a greatly decreased oxygen concentration from 31% for GOF and 5.8% for rGF to 1.5% for GF-HC. (**C**) HRTEM image of GF-HC. Inset: IFFT result of the HRTEM image revealing defect-free graphene honeycomb matrix. (**D**) HRTEM image of GF-HC exhibiting eight neighboring few-layered graphene sheets. (**E** and **F**) Cross-sectional SEM images of GF-HC revealing hierarchically connected gasbags and channels among graphene layers. (**G**) Top-view SEM image of GF-HC showing fissures in the graphene layers to serve as the vertical infiltration channel. (**H**) Top-view SEM images of GF-Hp illustrating the absence of fissures. (**I** and **J**) Infiltration demonstration of ionic liquid electrolyte on GF-HC in a glove box, suggesting a fast infiltration process.

Moreover, the electric resistance of GF-HC exhibited very few change when being folded at different angles (fig. S9B) and kept constant after 600 folding cycles (fig. S9C), revealing its excellent stability during bending operation (*10*).

Electrochemical performance of the GF-HC cathode

Owing to such a perfectly matched 3H3C design, the GF-HC cathode showed unprecedented electrochemical performances. At a high current density of 6 A g^{-1} (charge in 72 s; Fig. 3A), the GF-HC cathode afforded a high specific capacity of 120 mAh g^{-1} and Coulombic efficiency above 98% without activation cycles. After 16,000 cycles, the cathodic capacity was 100% retained. Significantly, the charge/discharge curves throughout these cycles almost overlapped, demonstrating excellent reversibility of the GF-HC cathode (Fig. 3B). By contrast, the less channeled GF-p cathode delivered a lower capacity of 70 mAh g^{-1} after 1000 activation cycles (Fig. 3A) that is comparable with graphitic cathode materials (*1*, *6*, *18*); the least channeled GF-Hp cathode delivered a very low specific capacity (<10 mAh g^{-1}). These comparisons suggest that the high channeling feature of GF-HC does upgrade electrochemical performances at both low and high rates (fig. S11, A to C) (*19*, *20*). Meanwhile, the capacity of GF-HC is also higher than that of defective GF-2500 (95 to 100 mAh g^{-1}; fig. S11E) and nonoriented yet high-quality graphene aerogel cathode (*2*), confirming the advantages of high-quality and high-orientation designs, respectively.

To further understand the mechanism of improved cathodic capacity, in situ XRD spectra of different cathodes were measured (Fig. 3C). Calculated by the *d*-spacing values of split (00*n* + 1) and (00*n* + 2) peaks (*21*, *22*), stage 3 intercalation was detected for the fully charged GF-HC cathode, whereas dominant stage 4 with small amount of stage 5 intercalation was detected for the fully charged GF-p cathode, and stage 4 intercalation for fully charged nonoriented graphene foam (*1*). This first observed full stage 3 intercalation state of charged GF-HC indicates average three adjacent graphene sheets between intercalant galleries, illuminating its more active sites and higher capacity than less channeling GF-p and stage 4 nonoriented graphene foam (average four adjacent graphene sheets between intercalant galleries) (*1*, *20*–*23*). The electrochemical impedance spectra (EIS; fig. S12) indicate that GF-HC exhibits a low ohmic resistance (10.96 ohms) almost equal to GF-p (11.1 ohms). However, the charge transfer resistance of GF-HC (1.61 ohms) is much lower than those of GF-p (3.124 ohms), GF-Hp (2516 ohms), nonoriented graphene foam (*2*), and only submillimeter continuous graphene powder (*24*), demonstrating its less interfacial resistance. These results indicate that the "3H3C" design facilitates both faster cathodic electrochemical reaction and higher anion intercalation degree (figs. S12 and S13).

Accordingly, the GF-HC cathode shows record electrochemical performances among all graphene cathodes of Al-ion battery. Constant specific discharge capacities, high Coulombic efficiency (>97%),

Downloaded from http://advances.sciencemag.org/ on January 19, 2021

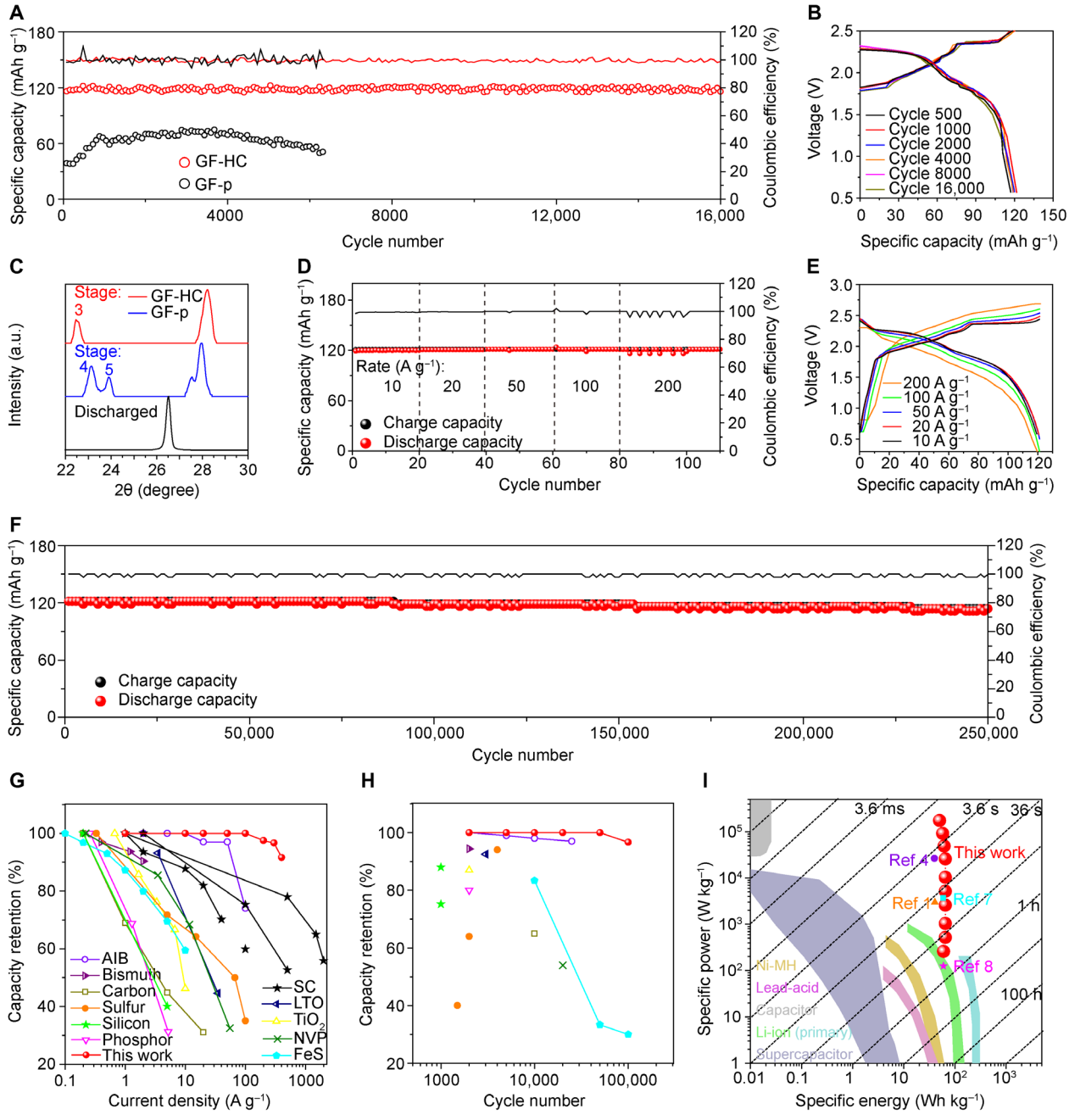


Fig. 3. Electrochemical performances. (**A**) Comparison of specific capacities between GF-HC and GF-p cathodes at 6 A g^{-1}. (**B**) Overlapped charge/discharge curves of the GF-HC cathode at different cycles, exhibiting two charging plateaus of 1.7 to 2.3 V and 2.3 to 2.5 V and two discharge plateaus of 2.3 to 2.0 V and 2.0 to 1.5 V, which correspond well with cyclic voltammetry in fig. S10. (**C**) In situ XRD results of fully charged GF-HC, GF-p, and fully discharged GF-HC cathodes. (**D**) Stable specific capacities of the GF-HC cathode at ultrahigh current densities from 10 to 200 A g^{-1} and (**E**) corresponding charge/discharge curves. (**F**) Stable cycling performance of the GF-HC cathode at current density of 100 A g^{-1} within 250,000 cycles. (**G** and **H**) Comparison of rate capability and cycle life characteristics between the GF-HC cathode and various research results. Legends of (H) are also listed in (G). Detailed data are listed in table S1 (*1*, *2*, *4*, *7*, *8*, *15*, *16*, *33*–*48*). (**I**) Comparison of the energy/power density of Al-GB with multiple commercialized energy storage technologies and various research results (*49*).

stable average discharge voltage, and low hysteresis were illustrated within wide range of current densities from 0.2 A g^{-1} (112 mAh g^{-1}; fig. S14, A and B) and 10 A g^{-1} (capacity of 121 mAh g^{-1} at 83 C, 1 C = 120 mA g^{-1}) to ultrahigh 200 and 300 A g^{-1} (116 mAh g^{-1} at 2500 C; Fig. 3, D and E, and fig. S14C). Notably, the GF-HC cathode still retained a reversible high capacity of 111 mAh g^{-1} at an extremely high current density of 400 A g^{-1} (~3333 C, charged in ~1.1 s) with clear charging/discharging plateau (fig. S14). This reveals ultrafast intercalation-based chemical redox reaction in the GF-HC cathode rather than physical adsorption-based electrical double-layer capacitive mechanism (*25*), which is consistent with the intercalation-based redox reaction mechanism demonstrated by in situ XRD spectra (Fig. 3C),

Downloaded from http://advances.sciencemag.org/ on January 19, 2021

well-separated redox peaks in cyclic voltammetry (CV) spectra (fig. S10A), and extremely low surface area (fig. S6). However, such an ultrahigh rate capability overwhelms those of all battery electrodes and is comparable with those of advanced supercapacitors. Benefiting from the high Young's modulus of the GF-HC cathode, ultralong cycling life is achieved at ultrahigh rate (for example, 100 A g^{-1}): 116 mAh g^{-1} after 100,000 cycles and 111 mAh g^{-1} after 250,000 cycles (Fig. 3F and figs. S11D and S14), which far surpasses those of previous battery materials. These excellent electrochemical performances, especially high-rate capability and ultralong cycle life (Fig. 3, G and H), promise a new generation of energy storage system (Fig. 3I) that can sustainably keep constant and stable energy density while providing high power delivery and uptake (energy density of ~66 Wh kg^{-1} with highest power density of 175 kW kg^{-1}).

Wide operation temperature range of Al-GB

Regarding real applications such as electric car operation in cold/hot climates or at high-altitude drones and tropical zone, low and high temperature electrochemical performances are fundamentally important in determining the pragmatic feasibility of an energy storage system (*7*, *26*). Benefiting from both ideal cathode design and thermal stability of ionic liquid electrolyte (*27*), the resulting Al-GB exhibits special superiority of stable cell performances at both high and low temperature (Fig. 4A) representing a pragmatic "all-climate battery." The GF-HC cathode afforded the same specific capacity and Coulombic efficiency at 60°C as those at 25°C. When the temperature was further enhanced to 80° or 100°C, stable discharge capacities (>115 mAh g^{-1}) with decreased Coulombic efficiency were found. To mitigate electrolyte decomposition and enhance the Coulombic efficiency (fig. S15), we applied a cutoff voltage optimization strategy to improve cycling stability (*2*, *21*). When the charge cutoff voltage was optimized to 2.44 V at 80°C, the GF-HC cathode showed neglectable decrease in specific capacity (119 to 117 mAh g^{-1}) yet high improvement in Coulombic efficiency (from 53 to 90%). Such a capacity can be 100% retained after 12,000 cycles with Coulombic efficiency above 97% (Fig. 4B). This cutoff voltage optimization strategy was also valid when the temperature

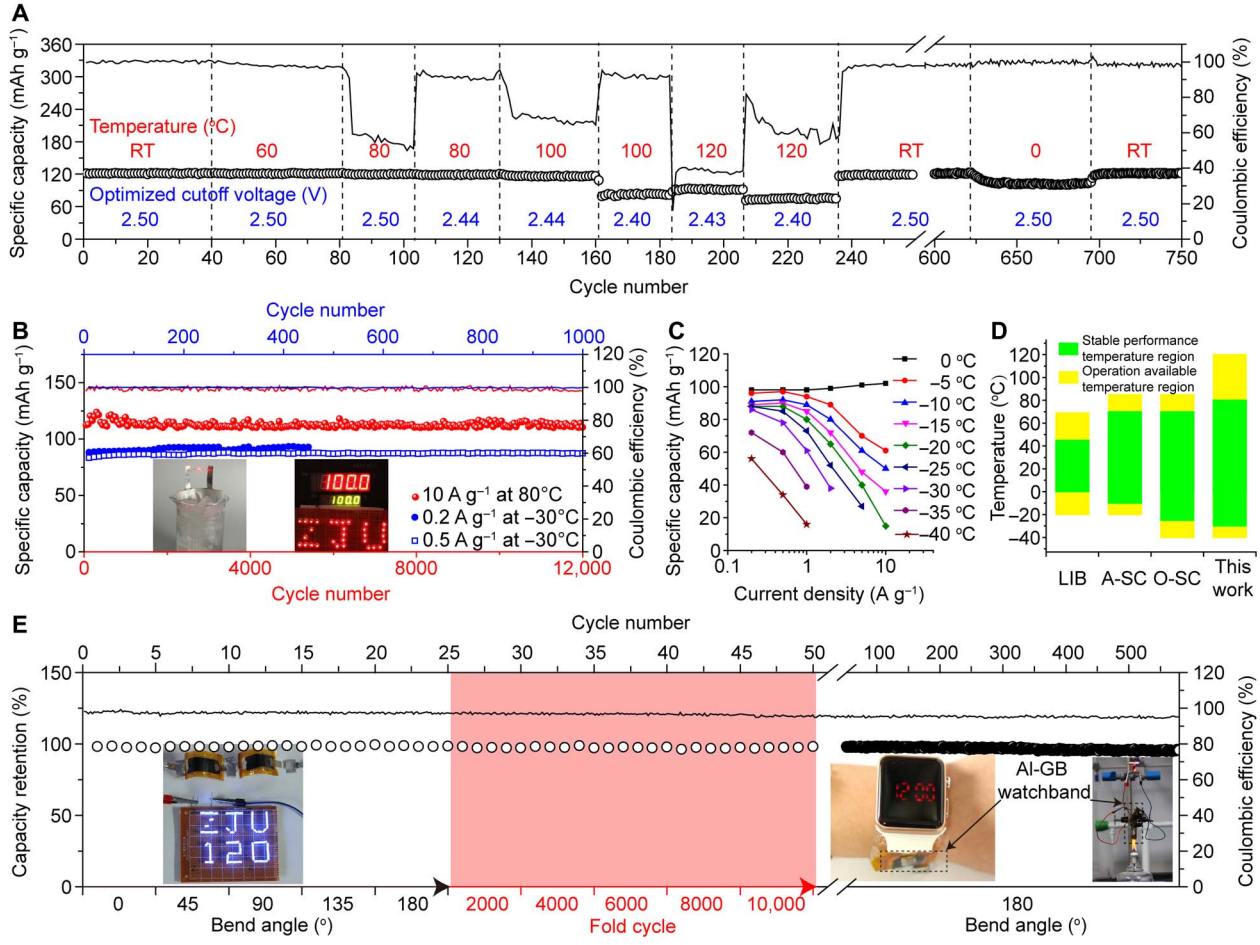


Fig. 4. Electrochemical performances of Al-GB at different temperatures and bending state. (**A**) Specific capacities and Coulombic efficiencies of GF-HC cathodes at different temperatures from 0 to 120°C with a cutoff voltage optimization strategy. RT, room temperature. (**B**) Stable cycling of the GF-HC cathode at 80°C (red, 12,000 cycles) and −30°C (blue, 1000 cycles). Inset: Al-GB soft pack cells successfully igniting LED lights in ice-salt bath and 100°C oven. (**C**) Summary of specific capacities and rate capability of the GF-HC cathode at different temperatures below 0°C. (**D**) Comparison of temperature range of Al-GB with multiple commercialized energy storage technologies of Li-ion battery (LIB), aqueous supercapacitor (A-SC), and organic supercapacitor (O-SC). (**E**) Stable cycling of Al-GB under different bending angles, and after 10,000 folding cycles (pink), followed by 500 battery cycles under 180° bending state. The capacity retention is calculated based on the cathode (120 mAh g^{-1}). Inset: Two bending Al-GB in series powering 65 LED lights (ignition voltage of 3.2 V) simultaneously; two flexible Al-GB serve as wearable watchband to power LED watch (ignition voltage of 3.5 V); the Al-GB watchband can still ignite red LED light for 1 min without explosion even when placed in the flame of alcohol lamp.

Downloaded from http://advances.sciencemag.org/ on January 19, 2021

was further enhanced to 100° or 120°C, achieving stable 45,000 cycles at 100°C (fig. S15E). The GF-HC cathode also afforded remarkable performance at low temperature: At 0° to −30°C, more than 70% of original capacity was retained, and even more than 55% capacity retention was achieved at −40°C (Fig. 4C and fig. S16). At −30°C, the GF-HC cathode still delivered specific capacity of higher than 85 mAh g^{-1} at 0.2 and 0.5 A g^{-1} with 100% capacity retention after 1000 cycles (Fig. 4B). By contrast, the GF-p cathode exhibited less capacity retention at low temperature due to less permeability (fig. S17). Hence, the excellent low temperature performance of Al-GB benefits not only from the high ionic conductivity of ionic liquid electrolyte (15 mS cm^{-1} at room temperature; fig. S16) but also from the unique 3H3C design of the GF-HC cathode (*7*, *28*). As a result, the Al-GB achieves a remarkable temperature endurance superior to those of lithium-ion battery (*29*, *30*) and supercapacitor (Fig. 4D) (*31*). This makes Al-GB applicable at wide temperature range. For instance, the Al-GB cell successfully ignited light-emitting diode (LED) lights under the ice-salt bath or 100°C baking (Fig. 4B).

Highly flexible Al-GB

Because of the flexible, continuous high electron-conducting electrodes, the Al-GB exhibited excellent flexibility for wearable energy storage application: The soft pack cell offered full capacity retention (117 mAh g^{-1} at 5 A g^{-1} based on the cathode, charged in 84 s) at different cell bending angles from 0° to 180° (fig. S18). This capacity was completely retained after both 10,000 times of 180° bending and following 500 battery cycles under 180° bending state. The EIS records also revealed almost no change in resistance after different bending cycles (fig. S19), supporting the stability of the flexible battery when being folded. Figure 4E shows two bent Al-GBs in series powering 65 blue LEDs (ignition voltage of 3.2 V) simultaneously for more than 5 min. These two Al-GBs further served as flexible watchbands to power the LED watch while wrapped around a human wrist (Fig. 4E and fig. S18, D to F). Moreover, in principle, Al-GB offers high safety due to incombustibility of all cell components (*2*). Even in the alcohol flame, the flexible Al-GB watchband kept igniting the LED light for 1 min without explosion (Fig. 4E).

DISCUSSION

Targeted 3H3C design is proposed to essentially resolve the "short slab" cathode problem of AIB, achieving high-performance Al-GBs with record rate capability, cycle life, and operation temperature range among all kinds of rechargeable batteries. Together with future innovation in low-cost electrolyte such as $[Et_3NH]Al_xCl_y$ (fig. S21), the emerging Al-GB provides a highly competitive choice for the capacitor-dominant high-power density energy storage system. In addition, the 3H3C design philosophy can also be extended to other electrode materials to effectively improve their electrochemical performances for practical electric power applications.

MATERIALS AND METHODS

Preparation of GF cathodes

First, commercially available GO solution (10 mg ml^{-1}; Hangzhou Gaoxi Technology Co. Ltd.) was casted on glass by a coating machine with controllable coating thickness, dried at room temperature, and then removed from the glass substrate to obtain GO film. Continuous fabrication of GO film was achieved by a classical wet-spinning method (*11*).

The rGO film was obtained by prereduction on GO film by N_2H_4 vapor at 90°C for 12 hours. Further high-temperature annealing treatment on rGO film in graphitization furnace (temperature raising rate of 500°C/hour under protection of argon flow) was used to prepare GF-2500 (annealed at 2500°C for 30 min without pressure), GF-HC (annealed at 2850°C for 30 min without pressure, density of 1.2 to 1.5 mg cm^{-3}), GF-p (annealed at 2850°C for 30 min with compression pressure of 0.2 kPa on GF), and GF-Hp (annealed at 2850°C for 30 min with compression pressure of 1 kPa on GF).

Preparation of electrolyte

The $[EMIm]Al_xCl_y$ electrolyte was prepared by mixing 1-ethyl-3-methylimidazolium chloride ([EMIm]Cl, 97%, Acros Chemicals, previously heated in vacuum at 130°C for 24 hours) with 1.3 mol equiv anhydrous aluminum chloride ($AlCl_3$, 99.999%; Sigma-Aldrich, use as bought) in a glove box for 12 hours to obtain transparent yellow liquid with viscosity as low as 6 centipoise and ionic conductivity of 15 mS cm^{-1} at 298 K.

The $[Et_3NH]Al_xCl_y$ electrolyte was prepared by mixing triethylamine hydrochloride (Et_3NHCl, 96%, Sigma-Aldrich, previously heated in vacuum at 110°C for 24 hours) with 1.5 mol equiv anhydrous aluminum chloride ($AlCl_3$, 99.999%, Sigma-Aldrich, use as bought) in a glove box for 12 hours to obtain transparent yellow liquid.

Electrochemical measurements

Coin cell was assembled with the GF cathode (used as prepared, areal loadings of GF-HC and control samples were fixed at 1 mg cm^{-2}), Al metal foil anode (thickness of 20 μm; MTI Corporation), nickel foam as the current collector of the cathode, glass fiber paper (thickness of 435 μm; Whatman 934-AH) as separator, and 50 μl of electrolyte. The absence of suspected side reactions (caused by stainless steel coin cell shell or nickel current collector) (*32*) is demonstrated in fig. S20. Soft pack cell was fabricated with the GF cathode, Al foil anode, nickel foil (or tantalum foil) for the current collector of the cathode, glass fiber paper as separator, and 200 μl of electrolyte. The flexible Al-GF battery was prepared by polyethylene terephthalate membrane coating battery core and then sealed with tapes. CV and EIS were performed on a CHI600D Electrochemical Workshop. The galvanostatic cycling measurements at room temperature were carried out on a Land BT2000 battery test system charged to 2.5 V (fig. S10). Battery performances at low and high temperatures were measured on MSK-TE906 battery temperature cycler.

Characterizations

The morphologies of the samples were investigated through a scanning electron microscope (Hitachi S-3000N) and a transmission electron microscope (JEM-2100F). The elemental mapping results were examined through an energy-dispersive spectrometer attached to Hitachi S-3000N. XRD data were collected on a Bruker D8 x-ray diffractometer with Cu Kα1 radiation (1.5405 Å) in a scan range of 10° to 80°. Raman spectra were obtained using an inVia-Reflex microRaman spectroscopy system with an excitation wavelength of 532 nm. The nitrogen adsorption-desorption isotherms were measured using a Quantachrome instrument (Autosorb-1-C) using vacuum-degassed samples (200°C for at least 6 hours). The isotherms were used to calculate (i) the specific surface area by the Brunauer-Emmett-Teller method and (ii) the pore volume and pore size by the Barrett-Joyner-Halenda method. XPS analysis was obtained on an ESCALAB 250Xi spectrometer with an Mg (Kα) source. Binding energies were calibrated

Downloaded from http://advances.sciencemag.org/ on January 19, 2021

using carbon (C1s = 284.6 eV). Contact angle measurements were conducted on HARKE-SPCA-1. Mechanical property tests were carried out on a HS-3002C equipped with a fine force detector. To examine the flexibility and durability of GFs, a cyclic bend test was conducted by HS-3002C, and the electrical conductivities of the GF during the bend tests were measured synchronously.

In situ XRD study of GF cathodes

In situ XRD study was achieved by the in situ battery mold. The battery was charged at a constant current density of 1 A g^{-1}. After fully charged (120 mAh g^{-1}), the battery was directly put on the x-ray diffractometer to obtain immediate results.

During the charging/anion-intercalation process, the (002) peak completely vanishes and splits into two new peaks. For a stage n graphite intercalation compound (GIC; the stage n of GICs is determined by the number of graphene layers between two intercalant layers), the most dominant peak is the $(00n + 1)$ and the second most dominant peak is the $(00n + 2)$. The d-spacing values of $(00n + 1)$ and $(00n + 2)$ peaks [that is, $d_{(n+1)}$ and $d_{(n+2)}$, respectively] can be calculated from XRD data by Bragg's equation (for example, Fig. 3C). By determining the ratio of the $d_{(n+2)}/d_{(n+1)}$ peak position and correlating these to the ratios of stage pure GICs, the most dominant stage phase of the observed GIC can be assigned (*21*).

For example, the fully charged GF-HC cathode exhibits two peaks at 22.52° and 28.22°, respectively. Their d-spacing values are 0.3942 and 0.3159 nm. The $d_{(n+2)}/d_{(n+1)}$ value is almost 1.25, which means stage 3 intercalation (*21*). The fully charged GF-p cathode shows four peaks: more split peaks at 23.14° and 27.93° exhibiting a $d_{(n+2)}/d_{(n+1)}$ value of 1.2, which means stage 4 intercalation, and less split peaks at 23.9° and 27.52° exhibiting a $d_{(n+2)}/d_{(n+1)}$ value of 1.15, which means stage 5 intercalation.

SUPPLEMENTARY MATERIALS

Supplementary material for this article is available at http://advances.sciencemag.org/cgi/content/full/3/12/eaao7233/DC1

fig. S1. Additional information for cathode material design, preparation, and characterizations.
fig. S2. Raman spectra, XRD patterns, and XPS spectra of GF-HC, GF-p, GF-Hp, and expanded graphite.
fig. S3. HRTEM images of expanded graphite and GF-HC.
fig. S4. SEM images of GF-HC, GF-p, and GF-Hp.
fig. S5. Orientation demonstration of GF-HC and graphene foam with statistic of cracks in different GF cathodes.
fig. S6. Porosity characteristics of GFs.
fig. S7. Permeability test of ionic liquid electrolyte on GF-HC and GF-Hp in a glove box.
fig. S8. Dynamic contact angle test of DMF droplet on different GF cathodes.
fig. S9. Mechanical properties of GF.
fig. S10. CV and cutoff voltage optimization of the GF-HC cathode.
fig. S11. Cycling performances of GF-HC and GF-p.
fig. S12. EIS and CV spectra of GF-HC, GF-p, GF-Hp, and graphite.
fig. S13. Element mapping of the charged GF-HC cathode.
fig. S14. Electrochemical performance of the GF-HC cathode at low rates.
fig. S15. Charge/discharge curves of the GF-HC cathode at different temperatures.
fig. S16. Charge/discharge curves of the GF-HC cathode and ionic conductivity of $[EMIm]Al_xCl_y$ ionic liquid electrolyte at low temperature.
fig. S17. Comparison of electrochemical performances of GF-HC and GF-p cathodes at low temperature.
fig. S18. Photograph of flexible Al-GB.
fig. S19. EIS spectra of flexible Al-GB soft pack cell after different bending cycles.
fig. S20. Additional information on coin cell fabrication, demonstration for the absence of side reaction, and the electrochemical performance based on mass loading.
fig. S21. Galvanostatic cycling of the GF-HC cathode with $[Et_3NH]Al_xCl_y$ electrolyte.
table S1. Electrochemical properties of electrode materials from various reports.
Calculations of $AlCl_4^-$ diffusivity based on CV plot
Calculations of $AlCl_4^-$ diffusivity based on EIS data
References (*50*, *51*)

REFERENCES AND NOTES

1. M.-C. Lin, M. Gong, B. Lu, Y. Wu, D.-Y. Wang, M. Guan, M. Angell, C. Chen, J. Yang, B.-J. Hwang, H. Dai, An ultrafast rechargeable aluminium-ion battery. *Nature* **520**, 324–328 (2015).
2. H. Chen, F. Guo, Y. Liu, T. Huang, B. Zheng, N. Ananth, Z. Xu, W. Gao, C. Gao, A defect-free principle for advanced graphene cathode of aluminum-ion battery. *Adv. Mater.* **29**, 1605958 (2017).
3. S. Jiao, H. Lei, J. Tu, J. Zhu, J. Wang, X. Mao, An industrialized prototype of the rechargeable Al/$AlCl_3$-[EMIm]Cl/graphite battery and recycling of the graphitic cathode into graphene. *Carbon* **109**, 276–281 (2016).
4. T. Lin, I.-W. Chen, F. Liu, C. Yang, H. Bi, F. Xu, F. Huang, Nitrogen-doped mesoporous carbon of extraordinary capacitance for electrochemical energy storage. *Science* **350**, 1508–1513 (2015).
5. J. Christensen, J. Newman, Stress generation and fracture in lithium insertion materials. *J. Solid State Electrochem.* **10**, 293–319 (2006).
6. Y. Wu, M. Gong, M.-C. Lin, C. Yuan, M. Angell, L. Huang, D.-Y. Wang, X. Zhang, J. Yang, B.-J. Hwang, H. Dai, 3D graphitic foams derived from chloroaluminate anion intercalation for ultrafast aluminum-ion battery. *Adv. Mater.* **28**, 9218–9222 (2016).
7. X. Yu, B. Wang, D. Gong, Z. Xu, B. Lu, Graphene nanoribbons on highly porous 3D graphene for high-capacity and ultrastable Al-ion batteries. *Adv. Mater.* **29**, 1604118 (2016).
8. D.-Y. Wang, C.-Y. Wei, M.-C. Lin, C.-J. Pan, H.-L. Chou, H.-A. Chen, M. Gong, Y. Wu, C. Yuan, M. Angell, Y.-J. Hsieh, Y.-H. Chen, C.-Y. Wen, C.-W. Chen, B.-J. Hwang, C.-C. Chen, H. Dai, Advanced rechargeable aluminium ion battery with a high-quality natural graphite cathode. *Nat. Commun.* **8**, 14283 (2017).
9. K. V. Kravchyk, S. Wang, L. Piveteau, M. V. Kovalenko, Efficient aluminum chloride–natural graphite battery. *Chem. Mater.* **29**, 4484–4492 (2017).
10. L. Peng, Z. Xu, Z. Liu, Y. Guo, P. Li, C. Gao, Ultrahigh thermal conductive yet super-flexible graphene films. *Adv. Mater.* **29**, 1700589 (2017).
11. Z. Liu, Z. Li, Z. Xu, Z. Xia, X. Hu, L. Kou, L. Peng, Y. Wei, C. Gao, Wet-spun continuous graphene films. *Chem. Mater.* **26**, 6786–6795 (2014).
12. Z. Xu, C. Gao, Graphene in macroscopic order: Liquid crystals and wet-spun fibers. *Acc. Chem. Res.* **47**, 1267–1276 (2014).
13. Z. Xu, Y. Liu, X. Zhao, L. Peng, H. Sun, Y. Xu, X. Ren, C. Jin, P. Xu, M. Wang, C. Gao, Ultrastiff and strong graphene fibers via full-scale synergetic defect engineering. *Adv. Mater.* **28**, 6449–6456 (2016).
14. X. Chen, W. Li, D. Luo, M. Huang, X. Wu, Y. Huang, S. H. Lee, X. Chen, R. S. Ruoff, Controlling the thickness of thermally expanded films of graphene oxide. *ACS Nano* **11**, 665–674 (2017).
15. C. Zhu, P. Kopold, P. A. van Aken, J. Maier, Y. Yu, High power–high energy sodium battery based on threefold interpenetrating network. *Adv. Mater.* **28**, 2409–2416 (2016).
16. J. Zhao, Y. Jiang, H. Fan, M. Liu, O. Zhuo, X. Wang, Q. Wu, L. Yang, Y. Ma, Z. Hu, Porous 3D few-layer graphene-like carbon for ultrahigh-power supercapacitors with well-defined structure–performance relationship. *Adv. Mater.* **29**, 1604569 (2017).
17. Z. Chen, W. Ren, L. Gao, B. Liu, S. Pei, H.-M. Cheng, Three-dimensional flexible and conductive interconnected graphene networks grown by chemical vapour deposition. *Nat. Mater.* **10**, 424–428 (2011).
18. G. Y. Yang, L. Chen, P. Jiang, Z. Y. Guo, W. Wang, Z. P. Liu, Fabrication of tunable 3D graphene mesh network with enhanced electrical and thermal properties for high-rate aluminum-ion battery application. *RSC Adv.* **6**, 47655–47660 (2016).
19. F. Shen, W. Luo, J. Dai, Y. Yao, M. Zhu, E. Hitz, Y. Tang, Y. Chen, V. L. Sprenkle, X. Li, L. Hu, Ultra-thick, low-tortuosity, and mesoporous wood carbon anode for high-performance sodium-ion batteries. *Adv. Energy Mater.* **6**, 1600377 (2016).
20. S. C. Jung, Y.-J. Kang, D.-J. Yoo, J. W. Choi, Y.-K. Han, Flexible few-layered graphene for the ultrafast rechargeable aluminum-ion battery. *J. Phys. Chem. C* **120**, 13384–13389 (2016).
21. G. Schmuelling, T. Placke, R. Kloepsch, O. Fromm, H.-W. Meyer, S. Passerini, M. Winter, X-ray diffraction studies of the electrochemical intercalation of bis(trifluoromethanesulfonyl)imide anions into graphite for dual-ion cells. *J. Power Sources* **239**, 563–571 (2013).
22. Y. Gao, C. Zhu, Z. Chen, G. Lu, Understanding ultrafast rechargeable aluminum-ion battery from first-principles. *J. Phys. Chem. C* **121**, 7131–7138 (2017).
23. J. Xu, Y. Dou, Z. Wei, J. Ma, Y. Deng, Y. Li, H. Liu, S. Dou, Recent progress in graphite intercalation compounds for rechargeable metal (Li, Na, K, Al)-ion batteries. *Adv. Sci.* **4**, 1700146 (2017).
24. H. Chen, C. Chen, Y. Liu, X. Zhao, N. Ananth, B. Zheng, L. Peng, T. Huang, W. Gao, C. Gao, High-quality graphene microflower design for high-performance Li–S and Al-ion batteries. *Adv. Energy Mater.* **7**, 1700051 (2017).

Downloaded from http://advances.sciencemag.org/ on January 19, 2021

25. P. Simon, Y. Gogotsi, B. Dunn, Where do batteries end and supercapacitors begin? *Science* **343**, 1210–1211 (2014).
26. C.-Y. Wang, G. Zhang, S. Ge, T. Xu, Y. Ji, X.-G. Yang, Y. Leng, Lithium-ion battery structure that self-heats at low temperatures. *Nature* **529**, 515–518 (2016).
27. A. A. Fannin, D. A. Floreani, L. A. King, J. S. Landers, B. J. Piersma, D. J. Stech, R. L. Vaughn, J. S. Wilkes, J. L. Williams, Properties of 1,3-dialkylimidazolium chloride-aluminum chloride ionic liquids. 2. phase transitions, densities, electrical conductivities, and viscosities. *J. Phys. Chem.* **88**, 2614–2621 (1984).
28. R. Lin, P.-L. Taberna, S. Fantini, V. Presser, C. R. Pérez, F. Malbosc, N. L. Rupesinghe, K. B. K. Teo, Y. Gogotsi, P. Simon, Capacitive energy storage from −50 to 100°C using an ionic liquid electrolyte. *J. Phys. Chem. Lett.* **2**, 2396–2401 (2011).
29. L. Lu, X. Han, J. Li, J. Hua, M. Ouyang, A review on the key issues for lithium-ion battery management in electric vehicles. *J. Power Sources* **226**, 272–288 (2013).
30. M.-T. F. Rodrigues, G. Babu, H. Gullapalli, K. Kalaga, F. N. Sayed, K. Kato, J. Joyner, P. M. Ajayan, A materials perspective on Li-ion batteries at extreme temperatures. *Nat. Energy* **2**, 17108 (2017).
31. G. Wang, L. Zhang, J. Zhang, A review of electrode materials for electrochemical supercapacitors. *Chem. Soc. Rev.* **41**, 797–828 (2012).
32. D.-J. Yoo, J.-S. Kim, J. Shin, K. J. Kim, J. W. Choi, Stable performance of aluminum-metal battery by incorporating lithium-ion chemistry. *ChemElectroChem* **4**, 2345–2351 (2017).
33. Y. Fang, L. Xiao, X. Ai, Y. Cao, H. Yang, Hierarchical carbon framework wrapped $Na_3V_2(PO_4)_3$ as a superior high-rate and extended lifespan cathode for sodium-ion batteries. *Adv. Mater.* **27**, 5895–5900 (2015).
34. C. Wang, L. Wang, F. Li, F. Cheng, J. Chen, Bulk bismuth as a high-capacity and ultralong cycle-life anode for sodium-ion batteries by coupling with glyme-based Electrolytes. *Adv. Mater.* **29**, 1702212 (2017).
35. S. Liu, J. Feng, X. Bian, J. Liu, H. Xu, Y. An, A controlled red phosphorus@Ni–P core@shell nanostructure as an ultralong cycle-life and superior high-rate anode for sodium-ion batteries. *Energy Environ. Sci.* **10**, 1222–1233 (2017).
36. H. Hou, C. E. Banks, M. Jing, Y. Zhang, X. Ji, Carbon quantum dots and their derivative 3D porous carbon frameworks for sodium-ion batteries with ultralong cycle life. *Adv. Mater.* **27**, 7861–7866 (2015).
37. S. Liu, Z. Wang, C. Yu, H. B. Wu, G. Wang, Q. Dong, J. Qiu, A. Eychmüller, X. W. Lou, A flexible TiO_2(B)-based battery electrode with superior power rate and ultralong cycle life. *Adv. Mater.* **25**, 3462–3467 (2013).
38. S. Chen, Y. Xin, Y. Zhou, Y. Ma, H. Zhou, L. Qi, Self-supported $Li_4Ti_5O_{12}$ nanosheet arrays for lithium ion batteries with excellent rate capability and ultralong cycle life. *Energy Environ. Sci.* **7**, 1924–1930 (2014).
39. S. Chen, L. Fan, L. Xu, Q. Liu, Y. Qin, B. Lu, 100 K cycles: Core-shell H-FeS@C based lithium-ion battery anode. *Energy Storage Mater.* **8**, 20–27 (2017).
40. N. Liu, Z. Lu, J. Zhao, M. T. McDowell, H.-W. Lee, W. Zhao, Y. Cui, A pomegranate-inspired nanoscale design for large-volume-change lithium battery anodes. *Nat. Nanotechnol.* **9**, 187–192 (2014).
41. S. Jing, H. Jiang, Y. Hu, J. Shen, C. Li, Face-to-face contact and open-void coinvolved Si/C nanohybrids lithium-ion battery anodes with extremely long cycle life. *Adv. Funct. Mater.* **25**, 5395–5401 (2015).
42. Y. Xu, Y. Wen, Y. Zhu, K. Gaskell, K. A. Cychosz, B. Eichhorn, K. Xu, C. Wang, Confined sulfur in microporous carbon renders superior cycling stability in Li/S batteries. *Adv. Funct. Mater.* **25**, 4312–4320 (2015).
43. Y. Qiu, W. Li, Z. Wen, G. Li, H. Yuan, M. Liu, L. Zhou, F. Ye, H. Li, Z. Wei, High-rate, ultralong cycle-life lithium/sulfur batteries enabled by nitrogen-doped graphene. *Nano Lett.* **14**, 4821–4827 (2014).
44. Y. Pan, Y. Zhou, Q. Zhao, Y. Dou, S. Chou, F. Cheng, J. Chen, H. K. Liu, L. Jiang, S. X. Dou, Introducing ion-transport-regulating nanochannels to lithium-sulfur batteries. *Nano Energy* **33**, 205–212 (2017).
45. Q. Pang, L. F. Nazar, Long-life and high-areal-capacity Li–S batteries enabled by a light-weight polar host with intrinsic polysulfide adsorption. *ACS Nano* **10**, 4111–4118 (2016).
46. K. Naoi, K. Kisu, E. Iwama, S. Nakashima, Y. Sakai, Y. Orikasa, P. Leone, N. Dupre, T. Brousse, P. Rozier, W. Naoi, P. Simon, Ultrafast charge–discharge characteristics of a nanosized core–shell structured $LiFePO_4$ material for hybrid supercapacitor applications. *Energy Environ. Sci.* **9**, 2143–2151 (2016).
47. C. Li, X. Zhang, K. Wang, X. Sun, G. Liu, J. Li, H. Tian, J. Li, Y. Ma, Scalable self-propagating high-temperature synthesis of graphene for supercapacitors with superior power density and cyclic stability. *Adv. Mater.* **29**, 1604690 (2017).
48. S. Li, C. Yu, J. Yang, C. Zhao, M. Zhang, H. Huang, Z. Liu, W. Guo, J. Qiu, A superhydrophilic "nanoglue" for stabilizing metal hydroxides onto carbon materials for high-energy and ultralong-life asymmetric supercapacitors. *Energy Environ. Sci.* **10**, 1958–1965 (2017).
49. P. Simon, Y. Gogotsi, Materials for electrochemical capacitors. *Nat. Mater.* **7**, 845–854 (2008).
50. A. C. Ferrari, J. C. Meyer, V. Scardaci, C. Casiraghi, M. Lazzeri, F. Mauri, S. Piscanec, D. Jiang, K. S. Novoselov, S. Roth, A. K. Geim, Raman spectrum of graphene and graphene layers. *Phys. Rev. Lett.* **97**, 187401 (2006).
51. J. Zhi, A. Z. Yazdi, G. Valappil, J. Haime, P. Chen, Artificial solid electrolyte interphase for aqueous lithium energy storage systems. *Sci. Adv.* **3**, e1701010 (2017).

Acknowledgments: We thank X. Yang and Z. Xu for assistance in contact angle test and the staffs in the Shanghai Synchrotron Radiation Facility for small-angle x-ray scattering characterizations. **Funding:** This work was supported by the National Natural Science Foundation of China (nos. 21325417, 51533008, and 51603183), National Key R&D Program of China (no. 2016YFA0200200), and Fundamental Research Funds for the Central Universities (nos. 2017QNA4036 and 2017XZZX008-06). **Author contributions:** C.G. and H.C. conceived and designed the research. H.C. and T.H. fabricated the electrode materials. H.C., H.X., S.W., and F.G. performed all electrochemical characterizations and analyzed the data. H.C., J.X., and S.C. wrote the manuscript with guidance from Z.X., W.G., and C.G. C.G. oversaw all research phases and revised the manuscript. All authors discussed and commented on the manuscript. **Competing interests:** The authors declare that they have no competing interests. **Data and materials availability:** All data needed to evaluate the conclusions in the paper are present in the paper and/or the Supplementary Materials. Additional data related to this paper may be requested from the authors.

Submitted 19 August 2017
Accepted 14 November 2017
Published 15 December 2017
10.1126/sciadv.aao7233

Citation: H. Chen, H. Xu, S. Wang, T. Huang, J. Xi, S. Cai, F. Guo, Z. Xu, W. Gao, C. Gao, Ultrafast all-climate aluminum-graphene battery with quarter-million cycle life. *Sci. Adv.* **3**, eaao7233 (2017).

Downloaded from http://advances.sciencemag.org/ on January 19, 2021

Science Advances

Ultrafast all-climate aluminum-graphene battery with quarter-million cycle life

Hao Chen, Hanyan Xu, Siyao Wang, Tieqi Huang, Jiabin Xi, Shengying Cai, Fan Guo, Zhen Xu, Weiwei Gao and Chao Gao

Sci Adv **3** (12), eaao7233.
DOI: 10.1126/sciadv.aao7233

ARTICLE TOOLS http://advances.sciencemag.org/content/3/12/eaao7233

SUPPLEMENTARY MATERIALS http://advances.sciencemag.org/content/suppl/2017/12/11/3.12.eaao7233.DC1

REFERENCES This article cites 51 articles, 3 of which you can access for free
http://advances.sciencemag.org/content/3/12/eaao7233#BIBL

PERMISSIONS http://www.sciencemag.org/help/reprints-and-permissions

Use of this article is subject to the Terms of Service

Science Advances (ISSN 2375-2548) is published by the American Association for the Advancement of Science, 1200 New York Avenue NW, Washington, DC 20005. The title *Science Advances* is a registered trademark of AAAS.

Copyright © 2017 The Authors, some rights reserved; exclusive licensee American Association for the Advancement of Science. No claim to original U.S. Government Works. Distributed under a Creative Commons Attribution NonCommercial License 4.0 (CC BY-NC).

Downloaded from http://advances.sciencemag.org/ on January 19, 2021